# Effect of pressure on transport and magnetotransport properties in $CaFe_2As_2$ single crystals

M. S. Torikachvili
*Department of Physics, San Diego State University, San Diego, California 92182-1233, USA*

S. L. Bud'ko, N. Ni, and P. C. Canfield
*Ames Laboratory U.S. DOE and Department of Physics and Astronomy, Iowa State University, Ames, Iowa 50011, USA*

S. T. Hannahs
*National High Magnetic Field Laboratory, 1800 East Paul Dirac Drive, Tallahassee, Florida 32310, USA*

(Received 25 May 2009; revised manuscript received 7 July 2009; published 24 July 2009)

The effects of pressure generated in a liquid-medium clamp pressure cell on the in-plane and *c*-axis resistance, temperature-dependent Hall coefficient, and low-temperature magnetoresistance in $CaFe_2As_2$ are presented. The $T-P$ phase diagram, including the observation of a complete superconducting transition in resistivity delineated in earlier studies is found to be highly reproducible. The Hall resistivity and low-temperature magnetoresistance are sensitive to different states/phases observed in $CaFe_2As_2$. Auxiliary measurements under uniaxial *c*-axis pressure are in general agreement with the liquid-medium clamp cell results with some difference in critical pressure values and pressure derivatives. The data may be viewed as supporting the potential importance of nonhydrostatic components of pressure in inducing superconductivity in $CaFe_2As_2$.

DOI: 10.1103/PhysRevB.80.014521 PACS number(s): 61.50.Ks, 74.62.Fj, 74.70.Dd, 74.25.Dw

## I. INTRODUCTION

In the recent hemorrhage of exciting experimental and theoretical results related to novel superconductivity in Fe-As containing materials, studies of $CaFe_2As_2$ take a rather special place. This compound was synthesized very recently in the form of large single crystals.[1–3] At ambient pressure, at ~170 K, a first-order structural [from high-temperature tetragonal (T) to low-temperature orthorhombic (O)] phase transition (with a few-degrees temperature hysteresis) was observed.[1] The structural phase transition was found to be coincident with an antiferromagnetic (AFM) ordering of Fe moments in the *ab* plane,[4] bearing similarity to $BaFe_2As_2$ and $SrFe_2As_2$.[5–10] The anisotropic three-dimensional magnetism in $CaFe_2As_2$ was further studied by inelastic neutron scattering and band-structure calculations.[11] Even more striking was the observation of pressure-induced superconductivity with $T_c \leq 12$ K observed in $CaFe_2As_2$ (Refs. 12 and 13) at very moderate, $P \sim 5$ kbar, pressures. Following the work on $CaFe_2As_2$, pressure-induced superconductivity was also found in $BaFe_2As_2$ and $SrFe_2As_2$,[14–19] albeit at significantly higher pressures. Neutron-scattering studies of the magnetic and structural properties of $CaFe_2As_2$ under hydrostatic (He gas and liquid-media cell) pressure[20] elucidated the complex $P-T$ phase diagram that has been roughly outlined as a result of electrical-transport measurements under pressure.[12] Three different magnetic/crystallographic phases were identified below room temperature under pressure up to ~6.5 kbar: in addition to nonmagnetically ordered T and antiferromagnetic O phases observed at ambient pressure,[4] a nonmagnetic "collapsed tetragonal" (cT) phase occurred in $CaFe_2As_2$ at low temperatures for pressures above ~3 kbar. This cT phase is stabilized by further increases in pressure rising to room temperature by ~17 kbar.[12,20] Band-structure calculations[20] confirmed the nonmagnetic character of the cT phase. Upon comparison with the phase diagram from transport measurements under pressure,[12] a conjecture that superconductivity dome appears in the nonmagnetic cT phase was proposed.[20] This picture appears to be in contradiction with the interpretation of the $\mu$SR experiments under pressure (using Daphne oil 7373 as a pressure medium) (Ref. 21) in which a coexistence of superconductivity with a magnetic order in a partial volume fraction was inferred. On the other hand, recent transport measurements under pressure (using silicone fluid as a pressure medium),[22] although confirming most of the results presented in Ref. 12, alleged that the extent of existence of the cT phase is limited by ~8 kbar below ~150 K with a new and unidentified phase located at higher pressures. (Later, after the appearance of several He pressure cell results,[20,23,24] the interpretation of the same set of data was significantly altered.[25]) In addition to aforementioned apparent dissimilarities in the interpretation of the experimental data, disparate views on the evolution of properties and ground states under pressure exist in band-structural results as well.[20,26,27] Finally, recent resistivity and magnetic-susceptibility measurements using helium as a pressure medium[23] have confirmed, but with *very sharp* features in resistivity, the phase lines associated with tetragonal to orthorhombic/antiferromagnetic as well as with tetragonal to the collapsed tetragonal phase transitions. However, no superconductivity was observed in either measurement leading to the conjecture[23,24] that a nonhydrostatic component of pressure is required to induce superconductivity in $CaFe_2As_2$.

The T to cT structural transition results in significant anisotropic change in the lattice parameters.[20] For $CaFe_2As_2$ in liquid-media pressure cells in the 5–10 kbar pressure range at the temperatures corresponding to T-cT transition the media is solid (polycrystalline or glass-like), so cooling through the structural transition may rather be thought of as a *constant-volume* not *constant-pressure* process.[23] It is clear then that in liquid-media cells, the $CaFe_2As_2$ sample is subjected to nonhydrostatic stresses on cooling through T-cT transition and the effect is magnified by large lattice parameters/

 

volume changes in the sample at this phase line. This results in multicrystallographic phase at low temperatures[24] and the superconducting dome observed in liquid-media pressure cells experiments, most probably, originates in one or another stressed crystallographic phase. A comprehensive overview of the physical properties of $CaFe_2As_2$ at ambient and high pressure is presented elsewhere.[28]

Given that He cells used have limited pressure ranges (generally below 7–10 kbar) and bearing in mind the somewhat limited and possibly contradictory results on $CaFe_2As_2$ under pressure, in this work we present a detailed study of magnetotransport in this material under pressure (in a liquid-medium clamp pressure cell) that is extending our previous results[12] supplemented by the data on the effect of uniaxial, along the $c$ axis, pressure on in-plane resistance in this material. The main goal of this study is to further explore the properties of $CaFe_2As_2$ under pressure generated in a pressure cell of a commonly used clamp type with a liquid medium so as to probe the superconducting state and conditions necessary to stabilize it.

## II. EXPERIMENTAL METHODS

Single crystals of $CaFe_2As_2$ were grown out of Sn flux (as discussed in Ref. 1 in more detail) using conventional high-temperature solution growth techniques.[29] Electrical transport and magnetotransport under pressure were measured for pressures below ~20 kbar generated in a Teflon cup filled with Fluorinert FC-75, with the cup inserted into a nonmagnetic piston-cylinder-type Be-Cu pressure cell with a core made of NiCrAl (40-KhNYu-VI) alloy. Pressure at low temperatures was determined by monitoring the $T_c$ of pure lead.[30] The pressure generation and medium was the same as that used in our previous publication.[12] For consistency, low-temperature pressure values will be used throughout the text. The uncertainty in pressure (~1 kbar for higher-temperature transitions) does not significantly affect our conclusions. The width of the superconducting transition in lead (together with the established $\Delta T_c(P)$ behavior[30] and bearing in mind smaller size of the sample in comparison to the Pb manometer) can be used to evaluate the pressure gradients in the cell at low temperatures. (Here, we ignore the fact that the Pb transition has a finite and very similar width at ambient pressure.) Figure 1 gives an estimate of $\Delta T_c = 0.02-0.03$ K, that could correspond to $\Delta P = 0.5-0.8$ kbar (or <5% at the higher end of our pressure range). This, though, is absolutely an upper limit to $\Delta P$ since a similar $\Delta T_c$ is found for the Pb manometer at ambient pressure as well. This estimate, however, does not address the very peculiar situation[23,28] caused by the cooling of the $CaFe_2As_2$ sample through a structural, tetragonal to collapsed-tetragonal, phase transition with a large *anisotropic* change in the lattice parameters[20,28] that almost invariably should cause an additional nonhydrostatic component of pressure, while the sample is constricted to the volume it occupied when the media froze.

The temperature and magnetic field environment for the pressure cell were provided by a Quantum Design Physical Property Measurement System (PPMS) instrument. The temperature of the sample was determined by an additional Cernox sensor attached to the body of the pressure cell. The cooling/warming rates were below 0.5 K/min. The resulting temperature lag between the Cernox on the body of the cell and the sample was <0.5 K at high temperatures and 0.1 K or less below ~70 K. For one of the samples ($I \| (ab), H \| c$) below ~10 K the resistivity was measured in 250 Oe field to suppress the superconductivity of traces of elemental Sn (residual flux).

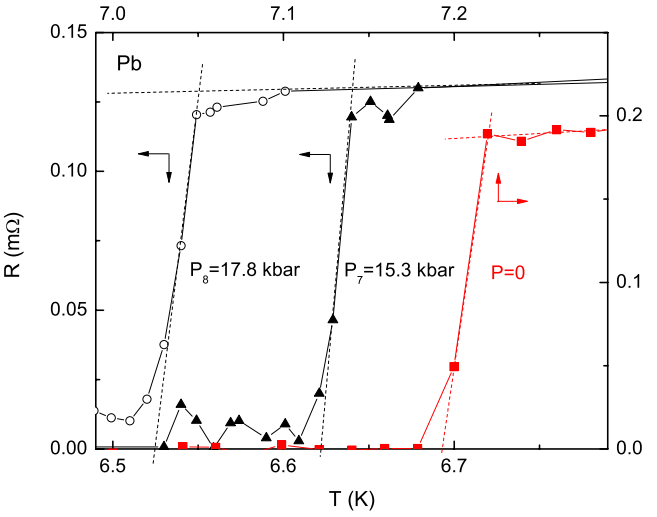


FIG. 1. (Color online) Example of resistive transitions in Pb, used as a low-temperature manometer, for two pressures above 15 kbar (left and bottom axes) and at $P=0$ (right and top axes). Dashed lines are guides for the eye.

Resistivity measurements under pressure in this work were performed for $H \| c$ orientation of the samples. The accuracy of the samples' orientation with respect to the applied field was ~5°. Pt wires and Epo-Tek H20E silver epoxy were used to make contact to the samples. For the $I \| (ab)$ sample the contacts were positioned in a standard linear geometry. For (semiquantitative) $I \| c$ measurements both current (larger) and voltage (smaller) contacts were positioned on the opposite parallel ($ab$) faces of the sample. In this case, the resulting resistivity has an admixture of both $\rho_{ab}$ and $\rho_c$ components, however, presumably, with a large contribution of the latter (c.f. Ref. 31). Hall measurements on $CaFe_2As_2$ under pressure were performed with current flowing in the $ab$ plane approximately parallel to the $a$ axis and field parallel to the $c$ axis. To eliminate the effect of a misalignment of the voltage contacts, the Hall measurements were taken for two opposite directions of the applied field, $H$ and $-H$, and the odd component, $[\rho_H(H)-\rho_H(-H)]/2$, was taken as the Hall resistivity. ±90 kOe magnetic fields were used for these measurements.

Additional field-dependent electrical-transport data under pressure for $CaFe_2As_2$ single crystal were collected using the 310 kOe resistive magnet in the National High Magnetic Field Laboratory in Tallahassee, FL with a $^3$He refrigerator insert that allowed for the accommodation of the pressure cell. For these measurements, electrical current was flowing in the $ab$ plane and the magnetic field was applied along the $c$ axis.

Resistance under uniaxial (along the $c$ axis) stress was measured in a home-made stress cell attached to a standard

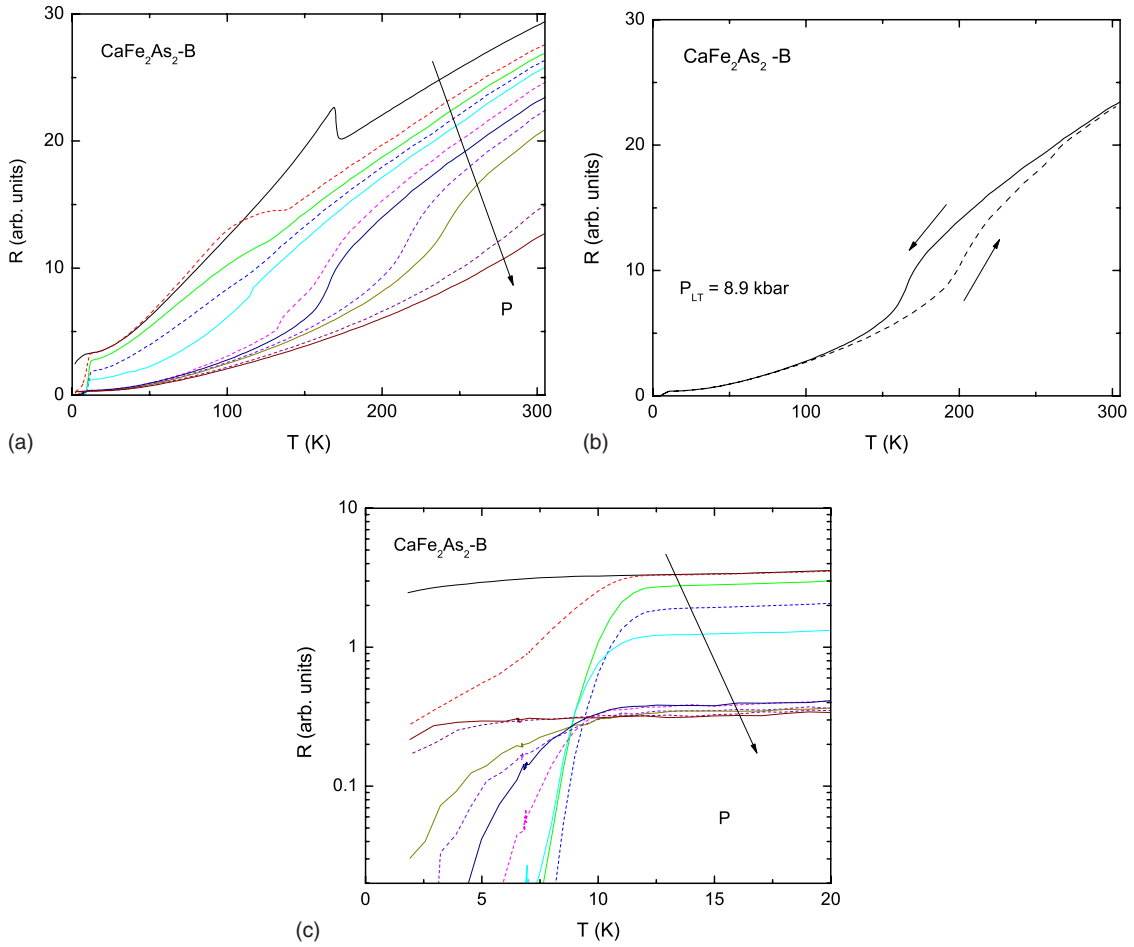


FIG. 2. (Color online) (a) Temperature-dependent in-plane resistance of $CaFe_2As_2$ at different applied pressure (0, 2.7, 4.3, 4.9, 6.4, 8.4, 8.9, 11.0, 12.1, 15.3, and 17.8 kbar; arrow is pointing in the direction of increase in pressure). Data taken on cooling are shown. (b) Data for $P=8.9$ kbar taken on cooling and warming. Panel (c): low-temperature part of the data in the panel (a). Room-temperature resistivity at ambient pressure is $\approx 280\ \mu\Omega$ cm.

PPMS puck. A rectangular uniformly thick sample was uniaxially compressed between two phosphor bronze disks with the surfaces in contact with the sample being electrically insulated. Thin and annealed platinum wires were used to make the electrical contacts to the sample in a standard four-probe geometry. The parts of the wires to be in contact with the sample were flattened before the experiment. (Mechanical contact under finite applied stress was enough to give contact resistances $\sim 1\ \Omega$ or less.) The body of the cell was made of phosphor bronze, the stress was applied via a NiCrAl spring that was calibrated (force vs compression) at room temperature using an Omega LCMDK-1KN load cell. There is an uncertainty in the temperature dependence of stress caused by difference in thermal expansions between phosphor bronze and the NiCrAl alloy and, more importantly, the change in elastic properties of the NiCrAl alloy on cooling. We are not aware of temperature-dependent elastic properties data for the NiCrAl alloy, however, for many steels and alloys the change in elastic constants from room temperature to liquid helium temperature is rather small, less than 20%,[32] so in the following we will use the room-temperature estimates for uniaxial pressure, $p_c=F/S$, where $S$ is the sample area. Given these approximations, the uniaxial stress is known (and controlled) at a semiquantitative level. In the following, (unless stated otherwise) the onset criterion is used to infer the superconducting transition temperature and the extremum (minimum) of the $d\rho/dT$ derivative is used to infer the structural/magnetic transitions temperatures.

## III. RESULTS AND DISCUSSION

Figure 2 presents the temperature-dependent resistance curves, $R(T)$, taken with current in the $(ab)$ crystallographic plane from sample B of $CaFe_2As_2$ (we denote the sample used in Ref. 12 as sample A). This set of data is in a very good agreement with our previous results[12] as well as with the results (but not the interpretation) of Lee *et al.*[22] The features associated with the T-O and T-cT phase transitions[12,20,22] are clearly seen in these data including the large, $\sim 30$ K, hysteresis at T-cT phase line [Fig. 2(b)] described in Ref. 12. A complete superconducting transition in resistance is observed for $4.3 \leq P \leq 11$ kbar with noticeable broadening of the transition above 6.4 kbar [Fig. 2(c)]. In addition to superconductivity being stabilized at intermediate pressures, Fig. 2(c) shows the very nonmonotonic drop in the

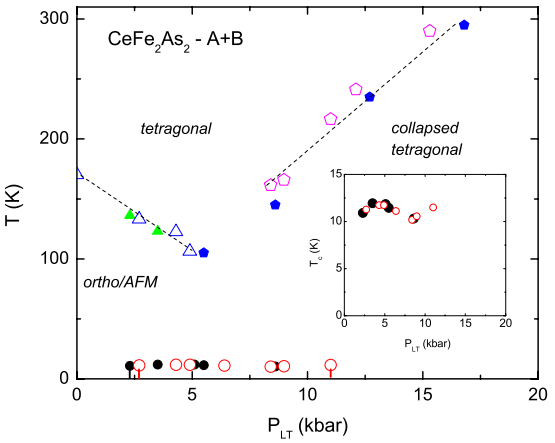


FIG. 3. (Color online) Combined phase diagram of $CaFe_2As_2$ under pressure. Open symbols: this work (sample B); filled symbols: previous data (Ref. 12) (sample A). Circles: onset of superconductivity; triangles: structural/AFM phase transition; and pentagons: T-cT phase transitions. Inset: enlarged $T_c(P)$ part of the phase diagram. Transition temperatures taken from $R(T)$ on cooling are shown. Dashed lines are guides for the eye.

residual resistivity with increasing pressure that has been associated with the superconducting region.[12]

The agreement between this work and our previous results is clearly seen in the combined phase diagram, Fig. 3, and in the pressure dependencies of the room-temperature and low-temperature normal-state resistivities, Fig. 4. The dramatic reduction in $\rho_{ab}$ found at 15 and 200 K is associated with the greatly reduced resistivity in the cT phase.[12,23] At 300 K the transition takes place at the far edge of our pressure range[12,24] and is hard to detect. It is worth noting the sizable pressure dependence of the T-phase resistivity above the cT transition. This is not unique to $CaFe_2As_2$ and is also large in $BaFe_2As_2$ and $SrFe_2As_2$.[18]

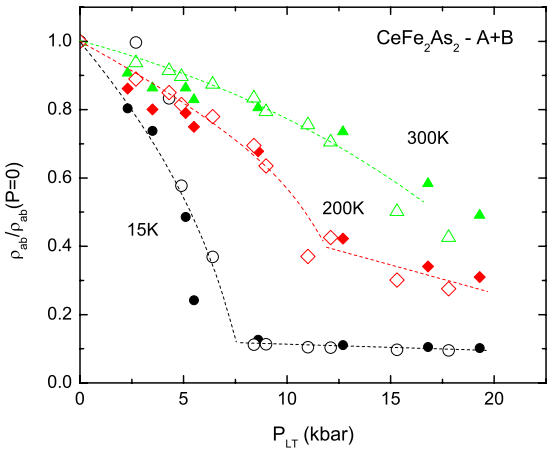


FIG. 4. (Color online) Normalized to the values at $P=0$ room-temperature in-plane resistivity, $\rho(300\ \mathrm{K})$, resistivity at 200 K, $\rho(200\ \mathrm{K})$, and low-temperature normal-state in-plane resistivity, $\rho(15\ \mathrm{K})$, for two samples of $CaFe_2As_2$ under pressure. Open symbols: this work (sample B); solid symbols: previous data (Ref. 12) (sample A). Dashed lines are guide to the eye.

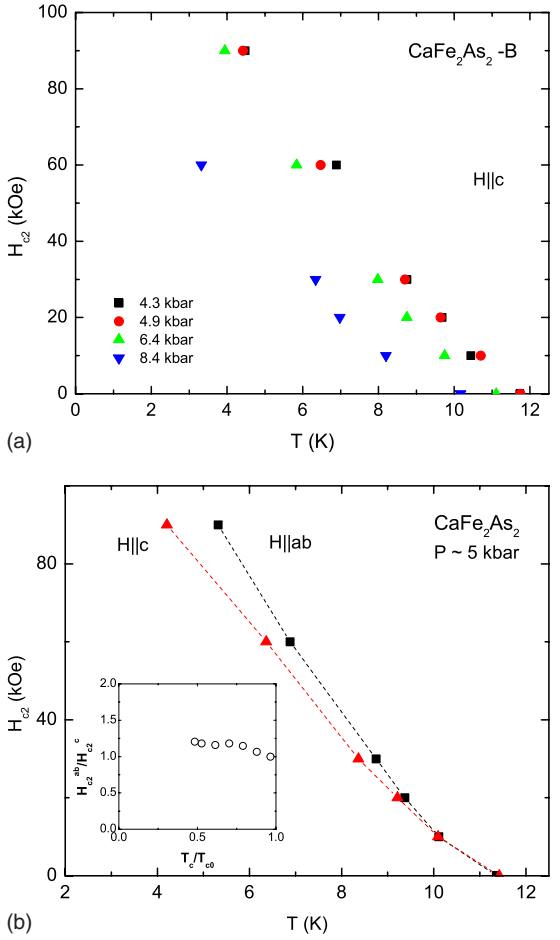


FIG. 5. (Color online) (a) Upper critical field, $H_{c2}(T)$, $(H\|c)$ of $CaFe_2As_2$, determined from the onset of resistive transitions at several values of pressure. (b) Anisotropic $H_{c2}(T)$ for $P\sim 5$ kbar: $P=5.5$ kbar for $H\|ab$ and average between 4.3 and 6.4 kbar for $H\|c$ are shown. Inset: estimate of the temperature-dependent anisotropy of the upper critical field in the pressure-induced superconducting phase in $CaFe_2As_2$ at $P\sim 5$ kbar.

Sample B was placed in the pressure cell so that $H\|c$ (as opposed to $H\|ab$ in our previous work[12]). The $H_{c2}(T)$ curves determined from the onsets of resistive transitions for several pressures are shown in Fig. 5(a). All of the curves have some upward curvature for low fields. A rough extrapolation suggests that the $H_{c2}(0)$ values range (for different pressures and models) between 70 and 140 kOe.

To evaluate the anisotropy of $H_{c2}$ in the pressure-induced superconducting phase of $CaFe_2As_2$, we combine the data sets for the two orientations of the applied field (obtained on two different samples) in Fig. 5(b). Since these data were obtained for two different samples in two different pressure runs, exactly the same pressures and $T_c(H=0)$ were not achieved. For a rough estimate of the anisotropy, we compare data for $P=5.5$ kbar for $H\|ab$ and average between 4.3 and 6.4 kbar $[T_c(H)=[T_c^{4.3\ \mathrm{kbar}}(H)+T_c^{6.4\ \mathrm{kbar}}(H)]/2]$ for $H\|c$. (This gives a zero-field $T_c$ closest to the 5.5 kbar data and allows for clearest estimate of anisotropy over widest field range.) The $H_{c2}$ anisotropy appears to be small, starting from $\sim 1$ close to $T_c(H=0)$ and increasing to $\sim 1.2$ at

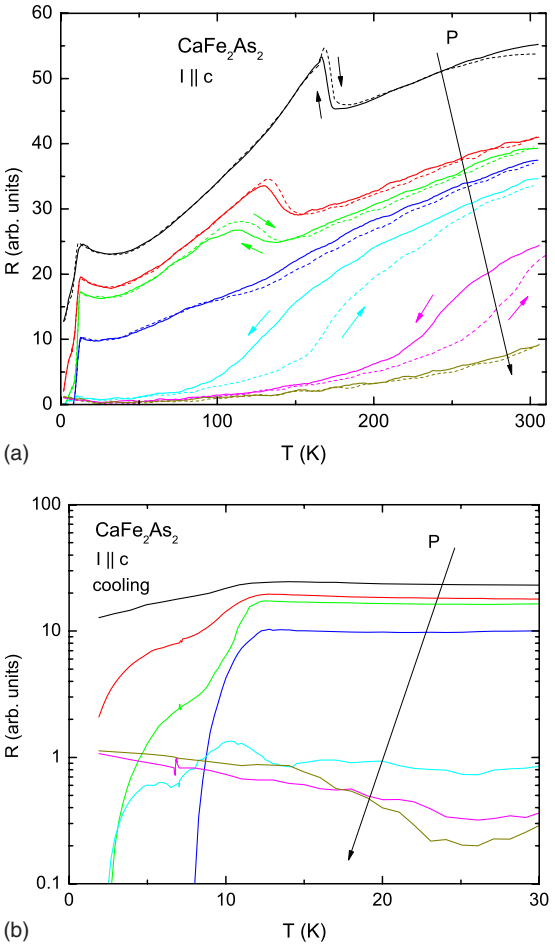


FIG. 6. (Color online) (a) Temperature-dependent resistance for $I \| c$ (see the text) of $CaFe_2As_2$ at different applied pressures (0, 2.0, 3.1, 4.3, 5.8, 12.0, and 17.4 kbar; arrow is pointing in the direction of increase in pressure). Data taken on cooling are shown as solid lines and that taken on warming are dashed lines. Panel (b): low-temperature part of the data in the panel (a) with only the data taken on cooling shown.

$T=1/2T_c(H=0)$. This $H_{c2}$ anisotropy is smaller than $\gamma \leq 6$ reported for $NdFeAs(O_{1-x}F_x)$,[33] and somewhat smaller, but similar to the $\gamma \leq 2$ found in K- or Co-doped superconducting $BaFe_2As_2$ crystals.[6,34–36] The $H_{c2}$ values in $CaFe_2As_2$ under pressure are approximately by factor of 2 lower than that in the $Ba(Fe_{1-x}Co_x)_2As_2$ samples with similar $T_c(H=0)$ at ambient pressure,[36] these difference may be due to the larger impurity scattering (i.e., shorter mean-free path) in the superconducting members of the $Ba(Fe_{1-x}Co_x)_2As_2$ series.

The temperature-dependent resistance curves at different pressures measured with the current flowing approximately along the $c$-crystallographic axis (both on cooling and on warming) are shown in Fig. 6(a). Taking into account the morphology of the $CaFe_2As_2$ crystals, possible errors on dimensions and the geometry of the contacts for these measurements, we can (conservatively) state that the anisotropy of resistivity in $CaFe_2As_2$ at ambient pressure is close to unity (within the factor of 2).[37] The structural/antiferromagnetic phase transition at ambient pressure is marked by an anomaly similar in form to that in in-plane

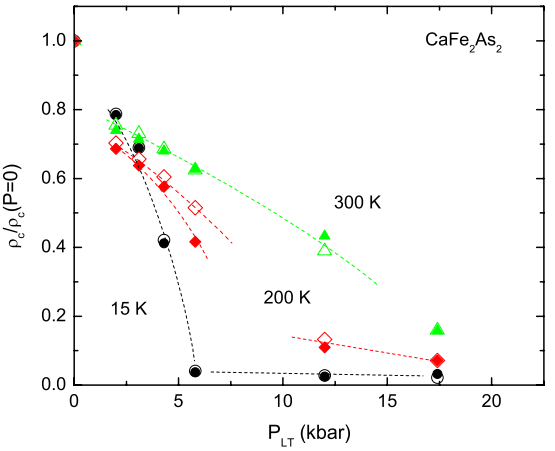


FIG. 7. (Color online) Normalized to the values at $P=0$ room-temperature resistivity, $\rho_c$(300 K), resistivity at 200 K, $\rho_c$(200 K), and low-temperature normal-state resistivity, $\rho_c$(15 K), for $CaFe_2As_2$ under pressure. Open symbols: data taken on warming; solid symbols: data taken on cooling.

resistivity $\rho_{ab}$. This anomaly moves down and broadens under pressure but remains, at comparable pressures, somewhat sharper than that seen for $\rho_{ab}$. At higher pressures, the tetragonal-to-collapsed-tetragonal phase transition is seen in $\rho_c(T)$ similar to the way it is observed in $\rho_{ab}(T)$. The hysteresis of the T-cT phase transition is again significantly larger than that for tetragonal-orthorhombic/AFM transition consistent with earlier observations.[12,22] A shallow minimum in the $c$-axis resistivity is seen at 20–30 K for all pressures studied. Finally, a sharp drop in $\rho_c(T)$ at $T \sim 10$ K is seen in $P=0$ and $P=2.0$ kbar data [Fig. 6(b)] possibly pointing to some incomplete filamentary superconductivity. For the next pressure, $P=3.1$ kbar, a complete, with $\rho=0$, superconducting transition (although with a low-temperature knee) is observed. At the next pressure (4.3 kbar) this transition is sharp and without a knee, then it broadens again at 5.8 kbar and is not seen at all at 12 kbar and higher.

The normal-state $c$-axis resistivity changes significantly under pressure (Fig. 7). The room-temperature resistivity decreases continuously under pressure and by $\sim$17 kbar becomes approximately factor of 6 smaller than at ambient pressure. For $3 \leq P \leq 6$ kbar, the resistivity at 15 K decreases rapidly down to $\sim$4% of its $P=0$ value and then, for higher pressures, practically does not change. This remarkable decrease in $\rho_c$ is the primary reason the high-pressure low-temperature resistivity data [Fig. 6(b)] appears to be so noisy (on a semilog plot). As was the case for $a$-axis resistivity, this rapid drop helps define the pressure range over which superconductivity is detected. Qualitatively, the behavior of the room-temperature and low-temperature normal-state $\rho_{ab}$ and $\rho_c$ resistivities under pressure is very similar, but with the relative changes in $\rho_c$ being larger. It should be noted that pressure may be promoting better connectivity between the sample layers and by this contributes to larger relative effect of pressure on $\rho_c$. As expected, the $\rho_c(T)$ data yield a $T-P$ phase diagram (Fig. 8) very similar to that obtained from $\rho_{ab}$ measurements (Ref. 12 and Fig. 3) (for comparison the phase lines inferred from data shown in Fig. 3 are also shown).

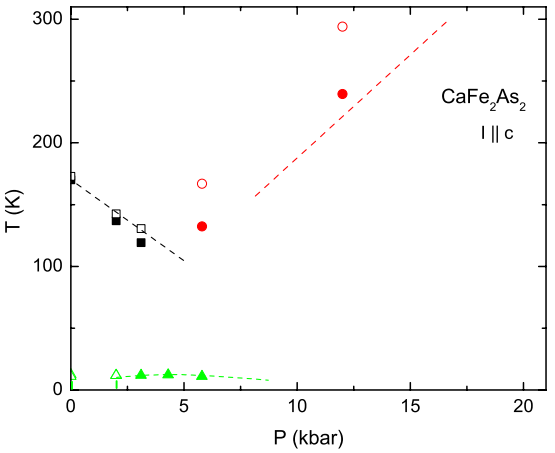


FIG. 8. (Color online) Pressure-temperature phase diagram of $CaFe_2As_2$ as obtained from temperature-dependent resistance for $I \| c$ (see text) measurements at different pressures. Solid triangles: onset $T_c$ for complete superconducting transitions; open triangles: for incomplete superconducting transitions; squares and circles: tetragonal-orthorhombic/AFM and tetragonal-collapsed-tetragonal phase transitions, respectively; solid symbols: on cooling; and open: on warming. Dashed lines: sketch phase boundaries from $I \| ab$ data in Fig. 3.

The temperature-dependent Hall coefficient, $\rho_H/H$ (where $\rho_H$ is the Hall resistance), measured for different applied pressures is plotted in Fig. 9. For an ambient pressure the data are similar to the earlier measurements.[2] As pressure is increased ($P=2.9$ and 3.5 kbar), the low-temperature downturn associated with orthorhombic/AFM phase becomes smaller and shifts to lower temperatures consistent with the $T-P$ phase diagram. For the 3.5 kbar curves, superconductivity (in the 90 kOe applied field used for the measurements) is signaled by the sharp low-temperature upturn (toward $\rho_H/H=0$) with the onset at $\sim 6$ K, grossly consistent

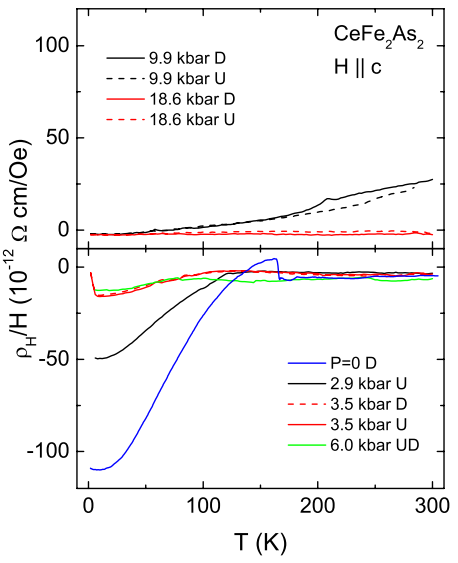


FIG. 9. (Color online) Temperature-dependent Hall coefficient $\rho_H/H$ measured at different pressures. Measurements on cooling and warming are marked "D" and "U," respectively, in the legend.

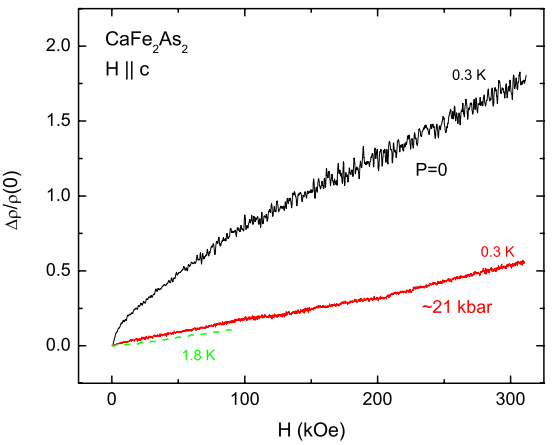


FIG. 10. (Color online) Normalized low-temperature ($T \approx 0.3$ K) magnetoresistivity at $P=0$ and $P \approx 21$ kbar for $CaFe_2As_2$. $I \| ab$ and $H \| c$. The even, MR, contribution plot for $P=21.2$ kbar; $T=1.8$ K is added (see Fig. 11 for more details.

with the $H_{c2}(T)$ data at different pressures in Fig. 5. The 9.9 kbar data show a signature associated with T-cT transition that is broad and hysteretic again consistent with the resistivity data [see Fig. 2(b) for a comparable data set]. It should be noted that the overall temperature behavior of 9.9 kbar curves is different from other sets of data, however one should have in mind that this is the only pressure at which the T-cT line is clearly crossed below room temperature. Finally, at 18.6 kbar the Hall coefficient is small and featureless, as one can expect for nonmagnetic normal metal. At low pressures, before crossing to the collapsed tetragonal phase, the evolution of the Hall coefficient of $CaFe_2As_2$ under pressure is qualitatively similar to that observed in $BaFe_2As_2$ with the electron doping in Fe site:[38–40] a shift in the anomaly associated with the structural/antiferromagnetic phase transition and a decrease in the absolute value of the low-temperature Hall coefficient, as opposed to the hole doping[38,41,42] results that show a change in sign of the low-temperature Hall coefficient. This similarity points out to the possibility of the effective electron doping (via similar changes in density of states/band structure) in $CaFe_2As_2$ under pressure in the low-pressure region.

The normal-state low-temperature ($T \approx 0.3$ K) magnetoresistivity (MR) was measured at ambient pressure (in the orthorhombic/AFM phase) and $P \approx 21$ kbar (in the collapsed tetragonal phase) with the current in the *ab* plane and magnetic field applied along the *c* axis (Fig. 10). Whereas no Shubnikov-de Haas oscillations were observed, the magnetoresistivity is rather high. The overall behavior changes from sublinear at ambient pressure to very close to linear at 21 kbar. To check if the linear odd in-field Hall contribution is not dominant in the observed magnetoresistivity behavior, measurements in positive and negative applied magnetic field for a sample with similar size, shape, orientation, and position of the contacts were made (Fig. 11). These 1.8 K data are similar to those shown in Fig. 9 for 0.3 K (see dashed line in Fig. 9) The even in magnetic field, magnetoresistive, component was observed to be significantly larger than the odd one, Hall component (see inset of Fig. 11),

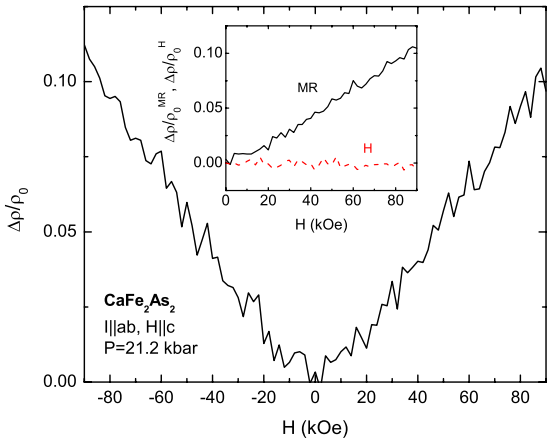


FIG. 11. (Color online) Normalized low-temperature ($T=1.8$ K) magnetoresistivity at $P=21.2$ kbar for $CaFe_2As_2$ ($I\|ab, H\|c$) measured in positive and negative applied magnetic field. Inset shows components of the field-dependent normalized resistivity even (MR) and odd (H) in magnetic field.

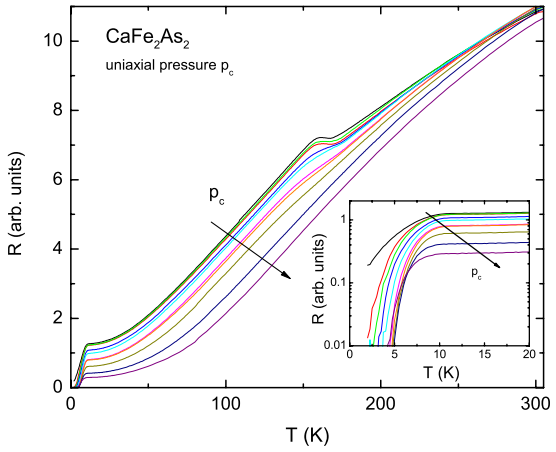


FIG. 12. (Color online) Temperature-dependent in-plane resistance of $CaFe_2As_2$ at different applied uniaxial pressures (0.5, 0.7, 0.8, 1.1, 1.4, 1.7, 2.1, 2.4, 2.7, 2.8 kbar; arrow is pointing in the direction of increase in pressure). Data taken on cooling are shown. Inset: low-temperature part of the data.

supporting the conclusion that the observed, close to linear, magnetoresistance of $CaFe_2As_2$ in the high-pressure collapsed tetragonal phase is not an artifact associated with add mixing in signal from the Hall component.

Naively, one would expect that, since (i) the low-temperature normal-state resistivity decreases by almost an order of magnitude under pressure and (ii) there is no magnetism (often considered as giving a negative contribution to the MR) in the cT phase, the normalized MR would be *higher* in the cT phase [e.g., by invoking Kohler's rule,[43–45] $\Delta\rho/\rho_0=F(H/\rho_0)$, where $\Delta\rho=\rho(T,H)-\rho(T,0)$ and $\rho_0=\rho(T,0)$]. In the experiment, it is more than a factor of 2 *lower* and its field dependence is greatly reduced and very close to linear. Linear MR itself is not a very common phenomenon. It was observed experimentally in some anisotropic semimetals (e.g., Refs. 44 and 45) as well as in bismuth films[46] and silver chalcogenides.[47] This phenomenon has attracted considerable theoretical attention[48] and is still a subject of discussions.[49] Even though the electronic anisotropy in the high-pressure collapsed tetragonal phase of $CaFe_2As_2$ is rather small, its rather low resistivity with a metallic, $d\rho/dT>0$, temperature dependence suggests that its linear low-temperature MR might share the common physics with that observed in other semimetals.[44–46] Clearly, more effort is required to address the origin of linear MR under pressure in $CaFe_2As_2$. The significant change in low-temperature MR in these materials under pressure brings attention to potentially interesting normal-state properties of $CaFe_2As_2$ and related Fe-As-based materials.

Given that nonhydrostatic components of pressure may be key to stabilizing superconductivity in $CaFe_2As_2$, preliminary measurements of in-plane resistance under uniaxial pressure applied along the $c$ axis were performed (Fig. 12). A complete ($R=0$) superconducting transition in resistance is observed already at $p_c\approx 0.7$ kbar, however, this transition is rather wide. The high-temperature feature associated with the structural/AFM transition at the ambient pressure broadens significantly under uniaxial pressure with a gradual suppression of its position (Fig. 13(a)). In the uniaxial pressure range of this study, the room-temperature (300 K) resistivity decreases only modestly at the highest pressures whereas low-temperature normal-state (15 K) resistivity decreases by almost a factor of 5 as uniaxial pressure is increased [Fig. 13(b)]. The overall behavior under uniaxial stress, $p_c$ is very similar to that under pressure in clamp piston-cylinder cell using liquid media. The slight difference is that a complete superconducting transition in resistivity is observed at significantly lower pressure leading to what appears to be a wide range of $p_c$ with apparent coexistence of superconductivity and magnetism. In order to make the comparison between our uniaxial and liquid-medium cell $T_c(P)$ data, the phase lines from Fig. 3 have been added to Fig. 13(a). Within our limited range of $p_c$ the agreement is noteworthy. It is possible that the low $p_c$ limit ($p_c<3$ kbar) in our measurements prevented the observation of the T-cT transition under uniaxial pressure, although, as will be discussed below, it is also possible that the cT phase does not appear under uniaxial pressure. Our uniaxial data suggest that the $c$-axis component of the pressure may be, to a large extent, responsible for the decrease in the magnetic/structural phase transition in $CaFe_2As_2$ and for the formation of the conditions for the observation of superconductivity in the resistivity measurements.

The superconducting transition, as seen in resistance, broadens significantly in applied field to the extent of becoming incomplete at $\sim 10$ kOe (Fig. 14, insets). This appears to be consistent with a small, just allowing for percolation in zero field, superconducting fraction. If, nevertheless, the onset of the transition is used to determine $H_{c2}(T)$ (Fig. 14), the results are similar to that obtained under liquid-medium ("hydrostatic") pressure.

## IV. SUMMARY

The results of this work show that the $P-T$ phase diagram of $CaFe_2As_2$ is robust and reproducible when measured in a liquid media and that the stabilized superconductivity mani-

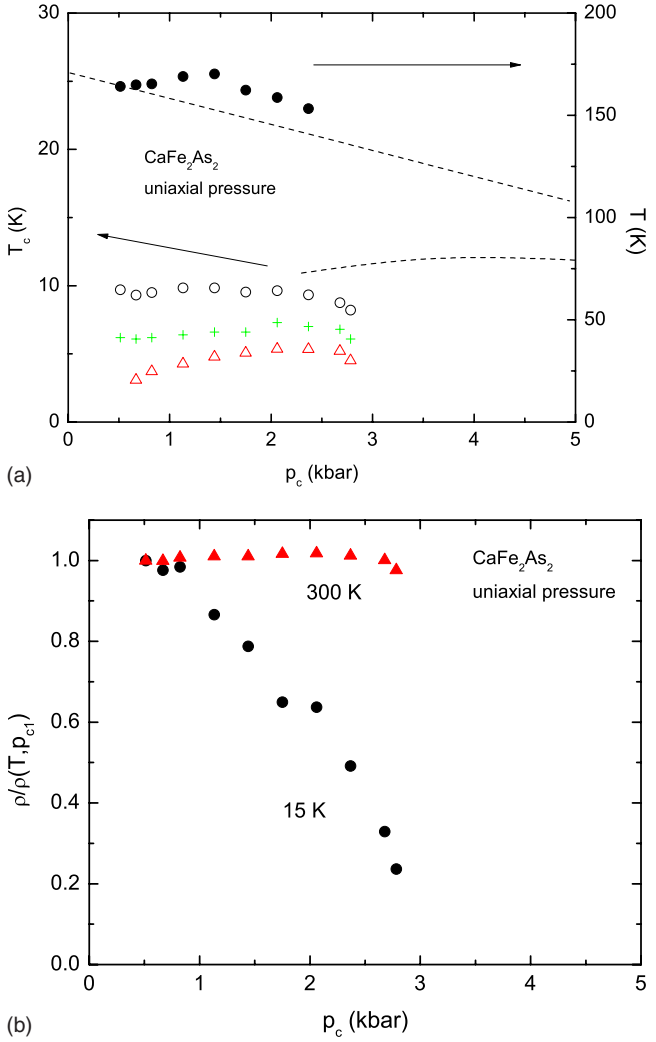


FIG. 13. (Color online) (a) Superconducting transition temperature (left axis) and structural/AMF transition temperature (right axis) as a function of uniaxial pressure. Symbols: circles: $T_c$ onset, triangles: $T_c$ offset, and crosses: maximum in $dR/dT$ derivatives; structural/AMF transition temperature was defined as a beginning of upturn in resistance (note that an alternative criterion, minimum in $dR/dT$ gives similar results). Dashed lines: sketches of the phase lines from liquid-medium cell measurements (Fig. 3). (b) Resistivity as a function of applied uniaxial pressure for $T=300$ K and $T=15$ K. Each curve is normalized to the lowest pressure value of the resistivity.

fests a similar, small, $H_{c2}(T)$ anisotropy as the other $AEFe_2As_2$ materials.[34–36] Phase diagrams assembled from resistivity measurements with current flowing along the *ab* plane or along the *c* axis are essentially identical and even when the $P-T$ phase diagram is determined using *c* axis uniaxial pressure there is good agreement, at least over the limited uniaxial pressure range available to us. It is noteworthy that the *c*-axis resistivity at room temperature appears to decrease faster than the in-plane resistivity (Fig. 15). If we assume the ambient-pressure resistivity anisotropy of approximately 2 found in Ref. 37, then the resistivity anisotropy decreases under pressure making the material even more three dimensional.

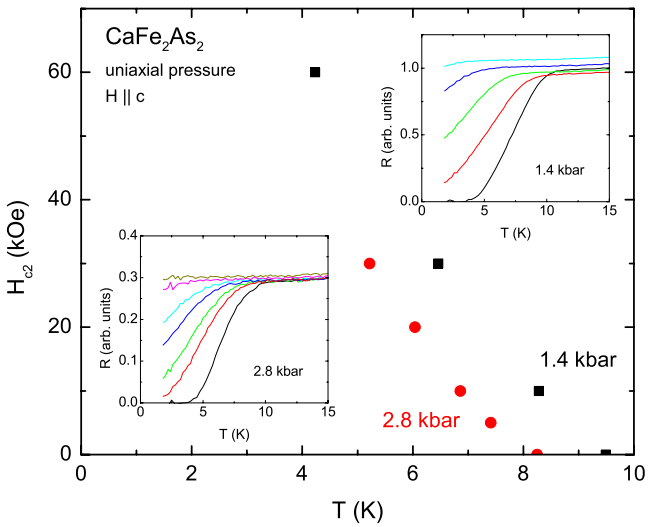


FIG. 14. (Color online) Temperature-dependent upper critical field ($H_{c2}$) determined at 1.4 and 2.8 kbar uniaxial pressures from the onsets of resistive transitions. Insets: low-temperature resistivities measured in different magnetic fields (0, 10, 30, 60, and 90 kOe for $p_c=1.4$ kbar and 0, 5, 10, 20, 30, 60, and 90 kOe for $p_c=2.8$ kbar) applied along the *c* axis.

Qualitatively, the evolution of Hall resistivity in $CaFe_2As_2$ under pressure is similar to that in $BaFe_2As_2$ with Co doping[38–40] in the lower pressure part of the $P-T$ phase diagram (suppression of the structural/AFM transition and observation of superconductivity). The current Hall data set, in the region of and above the T-cT transition, is somewhat sparse and may be affected by the multicrystallographic state of the sample at intermediate pressures and clearly requires further detailed studies. An apparent violation of the Kohler's rule in magnetoresistance under pressure for $CaFe_2As_2$ points out to significant difference in the band

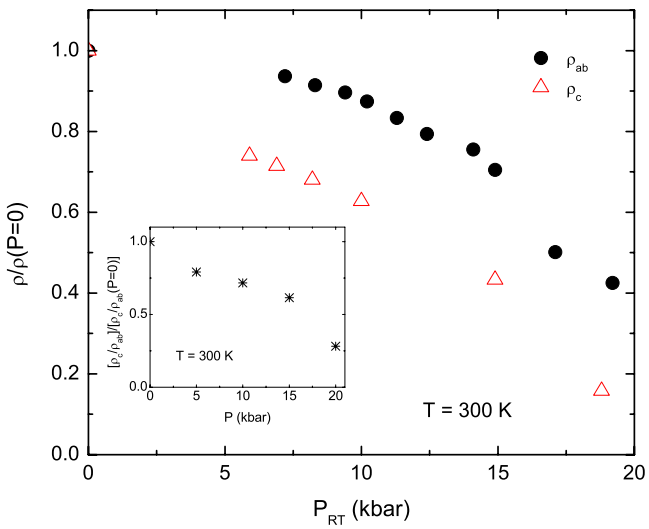


FIG. 15. (Color online) Normalized to the values at $P=0$ room-temperature resistivities, $\rho_{ab}(300\ \mathrm{K})$ and $\rho_c(300\ \mathrm{K})$ as a function of room-temperature values of pressure. Inset: estimate of the relative change in the room-temperature resistivity anisotropy under pressure.

structure and/or scattering between the low-temperature orthorhombic/AFM (at ambient pressure) and cT phase (at 19 kbar) that makes the Kohler's rule unapplicable. For the uniaxial *c*-axis pressure measurements, the existence of the T-cT phase line remains an open question. Either, given our relatively low maximum uniaxial pressure, we are just short of reaching the cT transition or, bearing in mind the drop in the low-temperature residual resistance, the uniaxial pressure could allow the system to bypass the cT phase by gradually changing the *c* axis and removing the driving force for the cT transition. The further uniaxial measurements should clarify this ambiguity.

## ACKNOWLEDGMENTS

Work at the Ames Laboratory was supported by the U.S. Department of Energy—Basic Energy Sciences under Contract No. DE-AC02-07CH11358. M.S.T. gratefully acknowledges support of the National Science Foundation under Grants No. DMR-0306165 and No. DMR-0805335. A portion of this work was performed at the National High Magnetic Field Laboratory, which is supported by NSF Cooperative Agreement No. DMR-0084173, by the State of Florida, and by the U.S. DOE.

[1] N. Ni, S. Nandi, A. Kreyssig, A. I. Goldman, E. D. Mun, S. L. Bud'ko, and P. C. Canfield, Phys. Rev. B **78**, 014523 (2008).
[2] F. Ronning, T. Klimczuk, E. D. Bauer, H. Volz, and J. D. Thompson, J. Phys.: Condens. Matter **20**, 322201 (2008).
[3] G. Wu, H. Chen, T. Wu, Y. L. Xie, Y. J. Yan, R. H. Liu, X. F. Wang, J. J. Ying, and X. H. Chen, J. Phys.: Condens. Matter **20**, 422201 (2008).
[4] A. I. Goldman, D. N. Argyriou, B. Ouladdiaf, T. Chatterji, A. Kreyssig, S. Nandi, N. Ni, S. L. Bud'ko, P. C. Canfield, and R. J. McQueeney, Phys. Rev. B **78**, 100506(R) (2008).
[5] M. Rotter, M. Tegel, D. Johrendt, I. Schellenberg, W. Hermes, and R. Pöttgen, Phys. Rev. B **78**, 020503(R) (2008).
[6] N. Ni, S. L. Bud'ko, A. Kreyssig, S. Nandi, G. E. Rustan, A. I. Goldman, S. Gupta, J. D. Corbett, A. Kracher, and P. C. Canfield, Phys. Rev. B **78**, 014507 (2008).
[7] R. Mittal, Y. Su, S. Rols, T. Chatterji, S. L. Chaplot, H. Schober, M. Rotter, D. Johrendt, and Th. Brueckel, Phys. Rev. B **78**, 104514 (2008).
[8] C. Krellner, N. Caroca-Canales, A. Jesche, H. Rosner, A. Ormeci, and C. Geibel, Phys. Rev. B **78**, 100504(R) (2008).
[9] J.-Q. Yan, A. Kreyssig, S. Nandi, N. Ni, S. L. Bud'ko, A. Kracher, R. J. McQueeney, R. W. McCallum, T. A. Lograsso, A. I. Goldman, and P. C. Canfield, Phys. Rev. B **78**, 024516 (2008).
[10] J. Zhao, W. Ratcliff, J. W. Lynn, G. F. Chen, J. L. Luo, N. L. Wang, J. Hu, and P. Dai, Phys. Rev. B **78**, 140504(R) (2008).
[11] R. J. McQueeney, S. O. Diallo, V. P. Antropov, G. D. Samolyuk, C. Broholm, N. Ni, S. Nandi, M. Yethiraj, J. L. Zarestky, J. J. Pulikkotil, A. Kreyssig, M. D. Lumsden, B. N. Harmon, P. C. Canfield, and A. I. Goldman, Phys. Rev. Lett. **101**, 227205 (2008).
[12] M. S. Torikachvili, S. L. Bud'ko, N. Ni, and P. C. Canfield, Phys. Rev. Lett. **101**, 057006 (2008).
[13] T. Park, E. Park, H. Lee, T. Klimczuk, E. D. Bauer, F. Ronning, and J. D. Thompson, J. Phys.: Condens. Matter **20**, 322204 (2008).
[14] Patricia L. Alireza, Y. T. Chris Ko, Jack Gillett, Chiara M. Petrone, Jacqueline M. Cole, Gilbert G. Lonzarich, and Suchitra E. Sebastian, J. Phys.: Condens. Matter **21**, 012208 (2009).
[15] K. Igawa, H. Okada, H. Takahashi, S. Matsuishi, Y. Kamihara, M. Hirano, H. Hosono, K. Matsubayashi, and Y. Uwatoko, J. Phys. Soc. Jpn. **78**, 025001 (2009).
[16] H. Kotegawa, H. Sugawara, and H. Tou, J. Phys. Soc. Jpn. **78**, 013709 (2009).
[17] A. Mani, N. Ghosh, S. Paulraj, A. Bharathi, and C. S. Sundar, arXiv:0903.4236v1 (unpublished).
[18] E. Colombier, S. L. Bud'ko, N. Ni, and P. C. Canfield, Phys. Rev. B **79**, 224518 (2009).
[19] Hisashi Kotegawa, Takayuki Kawazoe, Hitoshi Sugawara, Keizo Murata, and Hideki Tou, arXiv:0904.4631v1 (unpublished).
[20] A. Kreyssig, M. A. Green, Y. Lee, G. D. Samolyuk, P. Zajdel, J. W. Lynn, S. L. Bud'ko, M. S. Torikachvili, N. Ni, S. Nandi, J. B. Leão, S. J. Poulton, D. N. Argyriou, B. N. Harmon, R. J. McQueeney, P. C. Canfield, and A. I. Goldman, Phys. Rev. B **78**, 184517 (2008).
[21] T. Goko, A. A. Aczel, E. Baggio-Saitovitch, S. L. Bud'ko, P. C. Canfield, J. P. Carlo, G. F. Chen, Pengcheng Dai, A. C. Hamann, W. Z. Hu, H. Kageyama, G. M. Luke, J. L. Luo, B. Nachumi, N. Ni, D. Reznik, D. R. Sanchez-Candela, A. T. Savici, K. J. Sikes, N. L. Wang, C. R. Wiebe, T. J. Williams, T. Yamamoto, W. Yu, and Y. J. Uemura, Phys. Rev. B **80**, 024508 (2009).
[22] H. Lee, E. Park, T. Park, F. Ronning, E. D. Bauer, and J. D. Thompson, arXiv:0809.3550v1 (unpublished).
[23] W. Yu, A. A. Aczel, T. J. Williams, S. L. Bud'ko, N. Ni, P. C. Canfield, and G. M. Luke, Phys. Rev. B **79**, 020511(R) (2009).
[24] A. I. Goldman, A. Kreyssig, K. Prokeš, D. K. Pratt, D. N. Argyriou, J. W. Lynn, S. Nandi, S. A. J. Kimber, Y. Chen, Y. B. Lee, G. Samolyuk, J. B. Leão, S. J. Poulton, S. L. Bud'ko, N. Ni, P. C. Canfield, B. N. Harmon, and R. J. McQueeney, Phys. Rev. B **79**, 024513 (2009).
[25] H. Lee, E. Park, T. Park, F. Ronning, E. D. Bauer, and J. D. Thompson, arXiv:0809.3550v2 (unpublished).
[26] T. Yildirim, Phys. Rev. Lett. **102**, 037003 (2009).
[27] G. D. Samolyuk and V. P. Antropov, Phys. Rev. B **79**, 052505 (2009).
[28] P. C. Canfield, S. L. Bud'ko, N. Ni, A. Kreyssig, A. I. Goldman, R. J. McQueeney, M. S. Torikachvili, D. N. Argyriou, G. Luke, and W. Yu, Physica C **469**, 404 (2009).
[29] P. C. Canfield and Z. Fisk, Philos. Mag. B **65**, 1117 (1992).
[30] A. Eiling, and J. S. Schilling, J. Phys. F: Met. Phys. **11**, 623 (1981).
[31] C. Song, Jaehyun Park, Japil Koo, K.-B. Lee, J. Y. Rhee, S. L. Bud'ko, P. C. Canfield, B. N. Harmon, and A. I. Goldman, Phys. Rev. B **68**, 035113 (2003).
[32] H. M. Ledbetter, J. Appl. Phys. **52**, 1587 (1981); H. Ledbetter, Mater. Sci. Eng., A **442**, 31 (2006), and references therein.
[33] Y. Jia, P. Cheng, L. Fang, H. Luo, H. Yang, C. Ren, L. Shan, C.

Gu, and H.-H. Wen, Appl. Phys. Lett. **93**, 032503 (2008); Y. Jia, P. Cheng, L. Fang, H. Yang, C. Ren, L. Shan, C.-Z. Gu, and H.-H. Wen, Supercond. Sci. Technol. **21**, 105018 (2008).
[34] M. M. Altarawneh, K. Collar, C. H. Mielke, N. Ni, S. L. Bud'ko, and P. C. Canfield, Phys. Rev. B **78**, 220505(R) (2008).
[35] H. Q. Yuan, J. Singleton, F. F. Balakirev, S. A. Baily, G. F. Chen, J. L. Luo, and N. L. Wang, Nature (London) **457**, 565 (2009).
[36] N. Ni, M. E. Tillman, J.-Q. Yan, A. Kracher, S. T. Hannahs, S. L. Bud'ko, and P. C. Canfield, Phys. Rev. B **78**, 214515 (2008).
[37] M. A. Tanatar, N. Ni, G. D. Samolyuk, S. L. Bud'ko, P. C. Canfield, and R. Prozorov, Phys. Rev. B **79**, 134528 (2009).
[38] L. Fang, H. Luo, P. Cheng, Z. Wang, Y. Jia, G. Mu, B. Shen, I. I. Mazin, Lei Shan, Cong Ren, and Hai-Hu Wen, arXiv:0903.2418v2 (unpublished).
[39] F. Rullier-Albenque, D. Colson, A. Forget, and H. Alloul, arXiv:0903.5243v1 (unpublished).
[40] E. D. Mun, S. L. Bud'ko, N. Ni, and P. C. Canfield, arXiv:0906.1548v1 (unpublished).
[41] A. S. Sefat, D. J. Singh, L. H. VanBebber, Y. Mozharivskyj, M. A. McGuire, R. Jin, B. C. Sales, V. Keppens, and D. Mandrus, Phys. Rev. B **79**, 224524 (2009).
[42] S. L. Bud'ko, S. Nandi, N. Ni, A. Thaler, A. Kreyssig, A. Kracher, J.-Q. Yan, A. I. Goldman, and P. C. Canfield, arXiv:0906.4299v1 (unpublished).
[43] A. A. Abrikosov, *Fundamentals of the Theory of Metals* (North-Holland, Amsterdam, 1988).
[44] S. L. Bud'ko, P. C. Canfield, C. H. Mielke, and A. H. Lacerda, Phys. Rev. B **57**, 13624 (1998), and references therein.
[45] K. D. Myers, S. L. Bud'ko, I. R. Fisher, Z. Islam, H. Kleinke, and P. C. Canfield, J. Magn. Magn. Mater. **205**, 27 (1999).
[46] F. Y. Yang, Kai Liu, Kimin Hong, D. H. Reich, P. C. Searson, and C. L. Chin, Science **284**, 1335 (1999).
[47] M. Lee, T. F. Rosenbaum, M.-L. Saboungi, and H. S. Schnyders, Phys. Rev. Lett. **88**, 066602 (2002).
[48] A. A. Abrikosov, Phys. Rev. B **58**, 2788 (1998); Europhys. Lett. **49**, 789 (2000); J. Phys. A **36**, 9119 (2003), and references therein.
[49] Jingshi Hu and T. F. Rosenbaum, Nature Mater. **7**, 697 (2008).